HAL
open science

Chiroptical properties of 2,2'-bioxirane

Nicolas Daugey, Nicolas de Rycke, T. Brotin, T. Buffeteau

To cite this version:

Nicolas Daugey, Nicolas de Rycke, T. Brotin, T. Buffeteau. Chiroptical properties of 2,2'-bioxirane. Chirality, 2018, 30 (4), pp.342-350. 10.1002/chir.22814 . hal-01962169

HAL Id: hal-01962169

https://hal.science/hal-01962169v1

Submitted on 20 Dec 2018

HAL is a multi-disciplinary open access archive for the deposit and dissemination of scientific research documents, whether they are published or not. The documents may come from teaching and research institutions in France or abroad, or from public or private research centers.

L'archive ouverte pluridisciplinaire **HAL**, est destinée au dépôt et à la diffusion de documents scientifiques de niveau recherche, publiés ou non, émanant des établissements d'enseignement et de recherche français ou étrangers, des laboratoires publics ou privés.

Chiroptical Properties of 2,2'-Bioxirane

N. Daugey,[a] N. De Rycke,[b] T. Brotin,*[b] and T. Buffeteau*[a]

Abstract: The two enantiomers of 2,2'-bioxirane were synthesized and their chiroptical properties were thoroughly investigated in various solvents by polarimetry, vibrational circular dichroism (VCD), and Raman optical activity (ROA). Density functional theory (DFT) calculations at the B3LYP/aug-cc-pVTZ level revealed the presence of three conformers (G_+, G_- and *cis*) with Gibbs populations of 51, 44 and 5% for the isolated molecule, respectively. The population ratios of the two main conformers was modified for solvents exhibiting higher dielectric constants (G_- form decreases whereas G_+ form increases). The behavior of the specific optical rotation values with the different solvents was correctly reproduced by time-dependent DFT calculations using the polarizable continuum model (PCM), except for the benzene for which explicit solvent model should be necessary. Finally, VCD and ROA spectra were perfectly reproduced by the DFT/PCM calculations for the Boltzmann-averaged G_+ and G_- conformers.

Keywords: Bioxirane; conformational analysis; vibrational circular dichroism; Raman optical activity; DFT calculations

1 - INTRODUCTION

Small optically active oxiranes such as methyloxirane (also called propylene oxide) or epichloridrin are important precursors in organic synthesis. Independently of their use in organic chemistry, the chiroptical properties of oxirane derivatives are of great interest for researchers working in the field of chirality. Indeed, the low molecular weight of these compounds allows the study of their chiroptical properties under different experimental conditions. For instance, the chiroptical properties of small oxirane molecules, and in particular methyloxirane, have been thoroughly studied in the liquid state,[1-7] in the gas phase,[7,8] and even in the solid state (argon matrix)[9] by different techniques such as optical rotation dispersion (ORD), vibrational circular dichroism (VCD) and Raman optical activity (ROA). Moreover, methyloxirane has often been used as a model molecule in the development of VCD and OR theories.[3,10-15] Indeed, the simplicity of its chemical structure is a major asset to perform sophisticated quantum calculations at the density functional theory (DFT) level in presence (explicit solvation model) or not of solvent molecules.[6,16-21] Thus, large basis set can be used for DFT calculations allowing a prediction of its chiroptical properties with a high degree of accuracy. In addition, coupled cluster quantum calculations methods (such as CCSD), that require larger computational time, have been used to predict the chiroptical properties of different oxirane derivatives.[12,22-24]

Methyloxirane has also attracted great attention from the scientific community because it exhibits intriguing ORD curves in solution, resulting in a change of sign of the specific optical rotation (SOR) values in the nonresonant region.[25,26] Indeed, the SOR values of the (*S*)-methyloxirane are negative in the 300-600 nm region in benzene, CS_2 or dioxane solvents, positive in water, and negative/positive from long to short wavelengths in methanol or acetic acid solvents. Sophisticated DFT calculations were necessary to explain this strange behavior. For instance, it has been demonstrated that, solvent molecules surrounding enantiopure methyloxirane molecule adopt a chiral arrangement that can dominate the specific optical rotation (SOR) of the solute.[18] DFT calculations also show that the experimentally effects observed in water can be explained by considering methyloxirane-water clusters.[6]

Scheme 1. Chemical structure of (2*R*, 2'*R*)-2,2'-bioxirane, **R-1**

The interesting effects observed with methyloxirane prompted us to investigate in details the chiroptical properties of the two enantiomers of bioxirane (**1**). Our interest for this molecule is also motivated because bioxirane molecule could enter the cavity of cryptophane derivatives, which are molecular hosts synthesized in our group. To our knowledge the chiroptical properties of **1** have never been reported in the literature. This is probably because this molecule is not easy to synthesize and difficult to obtain commercially. In addition, bioxirane is harmful and must be handle with care.

Bioxirane contains two stereogenic centers and is composed of two oxirane cycles connected together by a single bond (Scheme 1). Thus, three stereoisomers are possible for this molecule: a couple of enantiomers (2*R*, 2'*R*)-**1** (**R-1**) and (2*S*, 2'*S*)-**1** (**S-1**), and a meso form (2*R*, 2*S* = 2*S*, 2*R*)-**1** (**M-1**) which is achiral. The two enantiomers of **1** have been prepared according to a procedure reported in the literature.[27] These two compounds have been isolated as crystals with a high enantiomeric purity suitable to perform chiroptical measurements.

In this article, we report the chiroptical properties of the two enantiomers of **1** in various solvents by polarimetry at several wavelengths, VCD, and ROA. Since **1** absorbs light in

[a] *Drs T. Buffeteau and N. Daugey*
Institut des Science Moléculaires, Bordeaux University
351, Cours de la Libération, 33405 Talence, France
E-mail: thierry.buffeteau@u-bordeaux.fr

[b] *Drs T. Brotin and N. De Rycke*
Ecole Normale Supérieure de Lyon, Lyon 1 University
46 Allée d'Italie, 69364 Lyon, France
E-mail: thierry.brotin@ens-lyon.fr

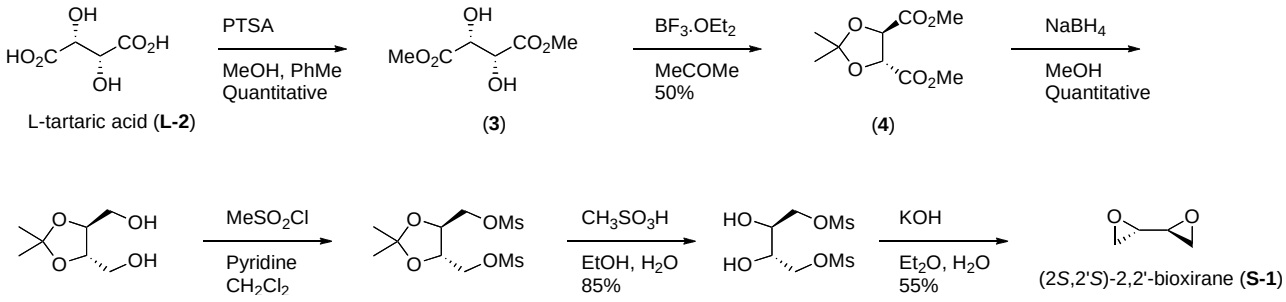

Scheme 2. Synthesis of (2*S*, 2'*S*)-2,2'-bioxirane (**S-1**) from L-(+)-tartaric acid (**L-2**)

the far UV region, its electronic circular dichroism (ECD) spectrum cannot be recorded with conventional ECD spectrometer and will not be investigated in this article. Quantum calculations at the DFT level (B3LYP/aug-cc-pVTZ) have been performed to predict the SOR values of the two enantiomers of **1** as well as their VCD and ROA spectra for different conformers of the bioxirane molecule.

2 – MATERIALS AND METHODS

2.1 – Polarimetric Measurements

Optical rotations of the two enantiomers of **1** were measured in various solvents (benzene, cyclohexane, carbon tetrachloride, chloroform, dichloromethane, dimethylformamide, acetonitrile, and water) at several wavelengths (589, 577, 546, 436, and 365 nm) using a polarimeter with a 10 cm cell thermostated at 25°C. Concentration used for the polarimetric measurements were typically in the range 1.3-3.4 g/100 mL.

2.2 – VCD Measurements

The infrared (IR) and VCD spectra were recorded on an FTIR spectrometer equipped with a VCD optical bench,[28] following the experimental procedure previously published.[29] In all the experiments, the photoelastic modulator was adjusted for a maximum efficiency at 1400 cm^{-1} (experiments in the fingerprint region) or at 3000 cm^{-1} (experiments in the CH stretching region). IR and VCD spectra were recorded at a resolution of 4 cm^{-1}, by coadding 50 and 24,000 scans (8h acquisition time), respectively. Samples were held in a 250 μm path length cell with BaF_2 windows. IR and VCD spectra of the two enantiomers of **1** were measured in CCl_4 and benzene-d_6 solvents at concentrations of 0.25 (fingerprint region) and 0.36 M (CH stretching region). Baseline corrections of the VCD spectra were performed by subtracting the raw VCD spectra of the solvent. Finally, in the presented IR spectra, the solvent absorption was subtracted out.

2.3 – ROA Measurements

Raman and ROA spectra were recorded on a ChiralRAMAN spectrometer, following the experimental procedure previously published.[30] The two enantiomers of **1** were dissolved in CCl_4, cyclohexane, benzene and water solvents at a concentration of 0.5 M and filled into fused silica microcell (4 × 3 × 10 mm). The laser power was 200 mW (~ 80 mW at the sample). The presented spectra in CCl_4 and cyclohexane are an average over about 55 h whereas those in water and benzene are an average over 22 h. Addition experiments were performed for the neat liquid.

2.4 – Theoretical calculations

Theoretical calculations were performed using the Gaussian09 package.[31] The possible stable conformers were searched by varying the C_1-C_2-C_4-C_5 dihedral angle giving rise to conformational flexibility, and optimizing these starting geometries at the B3LYP/aug-cc-pVTZ DFT level with or without the use of IEFPCM model of solvent.[32] Finally, three conformers were selected for further calculations.
Vibrational frequencies, IR and VCD intensities, and ROA intensity tensors (excitation at 532 nm) were calculated at the same levels of theory. For comparison to experiment, the calculated frequencies were scaled by 0.98 and the calculated intensities were converted to Lorentzian bands with a half-width at half-maximum (HWHM) of 4 cm^{-1}.
Optical rotation calculations have been carried out at several wavelengths (365, 436, 532, 546, 577 and 589 nm) using time-dependent DFT (TD-DFT) methods (B3LYP/aug-cc-pVTZ) as implemented in Gaussian09.

3 – RESULTS AND DISCUSSION

3.1 – Synthesis of (2*S*,2'*S*)-1 and (2*R*,2'*R*)-1

The enantiomer (2*S*, 2'*S*)-2,2'-bioxirane (**S-1**) was prepared from the commercially available (2*R*, 3*R*)-(+)-tartaric acid (L(+)-tartaric acid) (**2**), according to a known procedure (Scheme 2). The large-scale synthesis of (2*R*, 3*R*)-(+)-dimethyl tartrate (**3**) were performed by using the Fischer–Speier esterification conditions. In this study, benzene was replaced by toluene for safety reasons. The reaction provides compound **3** in quantitative yield.[33] Then, the acetal protection of diol was carried out using boron trifluoride etherate and acetone. The reaction gives rise to the enantiopure (4*R*,5*R*)-2,2-dimethyl-1,3-dioxolane-4,5-dicarboxylic acid dimethyl ester (**4**) in 50% yield.[34] Smooth conversion of enantiopure diesters to the corresponding diols was performed by using sodium borohydride to give rise to (4*S*, 5*S*)-(+)-2,2-dimethyl-1,3-dioxolane-4,5-dimethanol (**5**) in quantitative yield.[35] It is noteworthy that reproducibility problems were encountered when lithium alumino hydride was used instead of sodium borohydride. Compound **6**, was then obtained in 83 % yield by reacting compound **5** in presence of methanesulfonyl chloride in a mixture of pyridine and dichloromethane. The methanesulfonic acid-catalyzed deprotection of isopropylidene acetal moieties gives compound **7** in good yield (85 %). Finally, compound **S-1** was obtained from **7** by carrying out a double intramolecular nucleophilic substitution. The reaction was performed in a water/diethyl ether mixture in

presence of potassium hydroxide. The purification step of **S-1** (**CAUTION: very toxic product**) was performed by distillation under reduced pressure. This purification step allows us to obtain compound **S-1** as a white crystalline compound (mp: 22-23 °C) in 55% yield. The synthesis of the (2S, 2'S)-(-)-2,2'-bioxirane enantiomer was previously reported as an oily compound.[27] The synthesis of the enantiomer (2*R*, 2'*R*)-(-)-2,2'-bioxirane (**R-1**) was performed from (2*S*, 3*S*)-(-)-tartaric acid (D(-)-tartaric acid) using the same synthetic route (Supporting Information, Figure S1). Compound **R-1** was also isolated as a white crystalline compound (mp: 22-23 °C). The ^{1}H and ^{13}C NMR spectra of the two enantiomers of **1** are reported in Supporting Information (Figures S2-S5).

3.2 – Conformational analysis of R-1

To determine the more stable conformers of **R-1** enantiomer, we carried out a potential energy scan along the C_1-C_2-C_4-C_5 dihedral angle at the DFT level using the B3LYP functional and the aug-cc-pVTZ basis set. As shown in Figure 1, we identified two stable conformers G_+ and G_- at the C_1-C_2-C_4-C_5 dihedral angles 123.1° and -93.5°, respectively. The two conformers are separated by a barrier of almost 10 kJ mol^{-1} and differ in energy by 0.91 kJ mol^{-1}, corresponding to Boltzmann populations of 58%:40% at 293 K. A third minimum is observed at a dihedral angle of 23.6°, related to the *cis* conformation of the molecule. This conformer is however 8.31 kJ mol^{-1} higher in energy compared to G_+, corresponding to a Boltzmann population of 2%. The B3LYP equilibrium structures of the three conformers of **R-1**, as well as the C_1-C_2-C_4-C_5 dihedral angle are reported in scheme 3.

The geometry of the three conformers were re-optimized with the use of IEPCM model of solvent (cyclohexane, CCl_4, benzene, $CHCl_3$, CH_2Cl_2, CH_3CN, water).[32] The C_1-C_2-C_4-C_5 dihedral angles, the relative difference energies and populations based on the electronic (SCF) and the Gibbs free energies are listed in Table 1. Based on the ab initio Gibbs energies, the G_+ conformer is the most stable conformer regardless of the nature of the solvent and its contribution increases with the dielectric constant of the solvent (higher than 85 % in polar solvents). The contribution of the *cis* conformer is minor in all the calculations (lower than 4 %). Finally, it is noteworthy that the conformer exhibiting the higher calculated dipole moment is favored in the conformational distribution for polar solvents (Table S1).

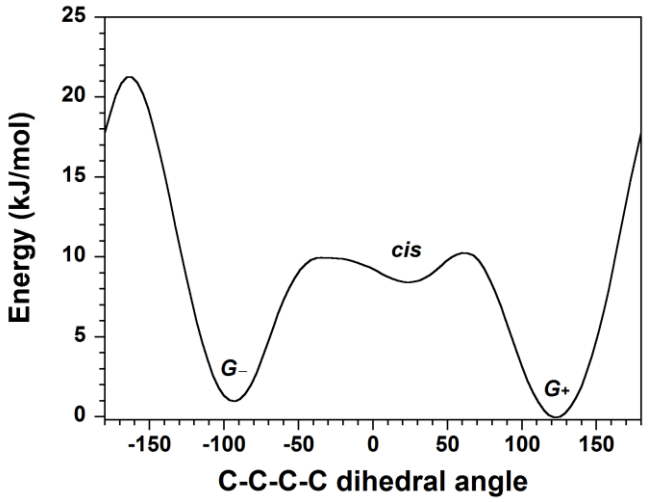

Figure 1. Potential energy scan of **R-1** along the C_1-C_2-C_4-C_5 dihedral angle (degree) (B3LYP/aug-cc-pVTZ)

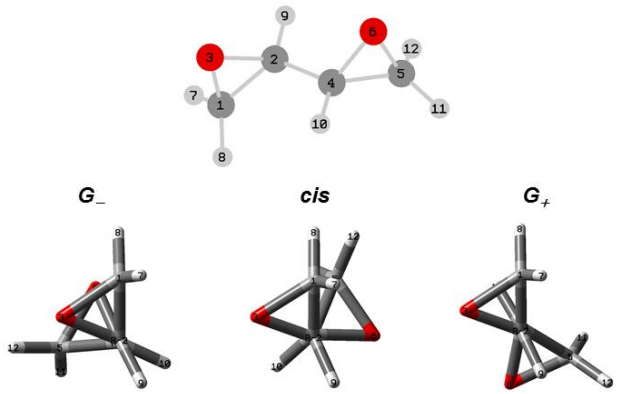

Scheme 3. B3LYP equilibrium structures of the three conformers of **R-1** (view along the C_2-C_4 bond)

Table 1. Conformations and energies of **R-1**

Solvent	type	dihedral angle [a]	SCF ΔE [b]	SCF Pop [c]	Gibbs ΔE [b]	Gibbs Pop [c]
vacuum	*cis*	23.6	8.31	2	5.84	5
	G_-	-93.5	0.91	40	0.37	44
	G_+	123.1	0	58	0	51
cyclohexane	*cis*	20.3	8.80	2	6.74	4
	G_-	-95.4	2.23	28	1.55	33
	G_+	124.4	0	70	0	63
CCl_4	*cis*	20.1	8.89	2	6.99	4
	G_-	-95.7	2.40	27	1.73	32
	G_+	124.5	0	71	0	64
benzene	*cis*	20.0	8.89	2	6.90	4
	G_-	-95.7	2.42	26	1.72	32
	G_+	124.6	0	72	0	64
$CHCl_3$	*cis*	19.2	9.66	1	7.61	3
	G_-	-97.2	3.34	20	2.52	25
	G_+	125.7	0	79	0	72
CH_2Cl_2	*cis*	19.2	10.07	1	9.66	2
	G_-	-98.3	3.85	17	4.50	13
	G_+	126.6	0	82	0	85
CH_3CN	*cis*	19.0	10.78	1	10.07	1
	G_-	-99.4	4.30	14	4.83	12
	G_+	127.4	0	85	0	87
water	*cis*	19.0	10.78	1.	10.23	1
	G_-	-99.7	4.39	14	4.90	12
	G_+	127.6	0	85	0	87

[a] C_1-C_2-C_4-C_5 dihedral angle in degrees. [b] Relative difference energies in kJ mol^{-1}. [c] Percent population.

3.3 – Chiroptical properties of 1

3.3.1 – Polarimetry of R-1 and S-1

The two enantiomers of **1** are well soluble in most of the organic solvents and in water. Thus, polarimetric experiments were performed in benzene, cyclohexane (sparingly soluble), tetrachloromethane (CCl_4), chloroform ($CHCl_3$), dichloromethane (CH_2Cl_2), acetonitrile (CH_3CN) and water. The SOR values of **R-1** and **S-1** are reported in Supporting Information (Table S2) and their wavelength dependences are presented in Figure 2 for **R-1**. The SOR values of **R-1** are negative in the nonresonant region (350 – 600 nm) regardless of the wavelengths and the nature of the solvent. Similar SOR values were obtained in CH_3CN and CH_2Cl_2 solvents. Weaker values were measured for nonpolar solvents such as cyclohexane, CCl_4 and $CHCl_3$, whereas slightly higher values were measured in water. Surprisingly, the SOR values measured in benzene are three times higher than those measured in the other solvents.

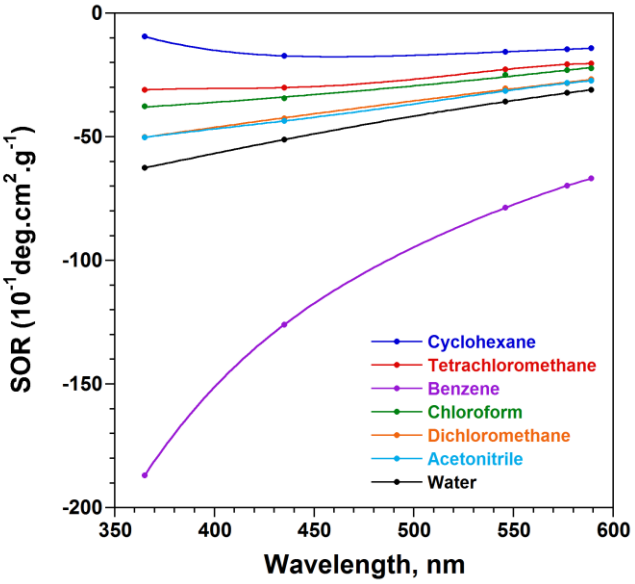

Figure 2. Specific optical rotation values (10^{-1} deg cm^2 g^{-1}) of **R-1** recorded at several wavelengths (365, 435.8, 546.1, 577 and 589 nm) in cycloxexane (c = 2.8), tetrachloromethane (c = 1.6), chloroform (c = 2.5), dichloromethane (c = 1.3), acetonitrile (c = 3.3), water (c = 3.2) and benzene (c = 2.6) solvents.

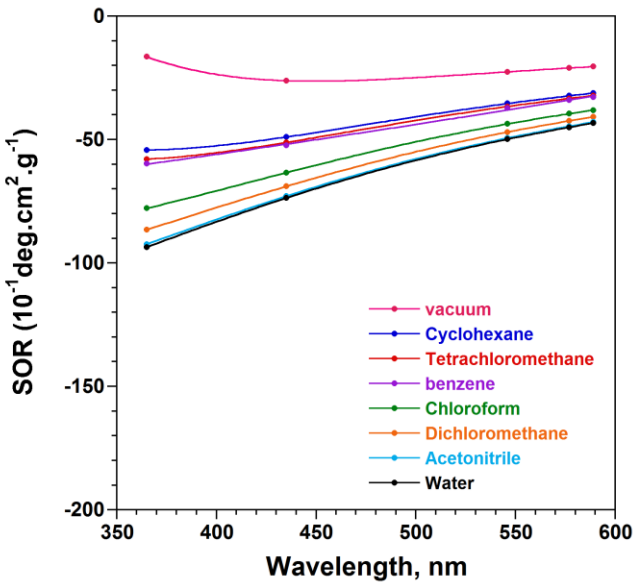

Figure 3. Specific optical rotation values (10^{-1} deg cm^2 g^{-1}) of **R-1** calculated at the B3LYP/aug-cc-pVTZ level in vacuum and using the IEFPCM model of solvent for several wavelengths (365, 435.8, 546.1, 577 and 589 nm).

To explain the SOR behavior as a function of the nature of the solvent, we have calculated the SOR values at the B3LYP/aug-cc-pVTZ TD-DFT level with the use of IEFPCM model of solvent. The calculations were performed for the three conformers of **R-1** (Figures S6 in the Supporting Information) as well as for the composition of conformers derived from SCF energies (Figure 3). For the G_- conformer, the SOR values are positive in the 350 – 600 nm region regardless of the solvent, but they decrease when the dielectric constant of the solvent increases. An opposite behavior is obtained for the G_+ conformer. This feature is interesting since the opposite behavior involves only a change of the conformation of the bioxirane molecule and not a change of its absolute configuration. Finally, for the *cis* conformer, positive SOR values were calculated with no significant differences regardless of the nature of the solvent. However, the SOR values are almost four times higher than for the two other conformers. Interestingly, these theoretical calculations suggest that even a small change in the population of the three conformers depending on the nature of the solvent could have a significant impact on the SOR values.

As shown in Figure 3, the SOR curves predicted considering the relative populations of the three conformers, reproduce fairly well the behavior of the experimental SOR curves measured for the for the CCl_4, $CHCl_3$, CH_2Cl_2, CH_3CN and H_2O solvents. Indeed, negative SOR values were calculated whatever the solvent used, with more negative values when the dielectric constant of the solvent increases. Since only electrostatic solute-solvent interactions are included in the IEFPCM model, our results shows that, for these four solutions, electrostatic effects are dominant. In contrast, a disagreement is observed between experimental and predicted SOR values for the cyclohexane and the benzene solutions It is interesting to note that this disagreement occurs for the two solvents exhibiting the largest molecular sizes. For the cyclohexane solution, the experimental SOR curve seems to be correctly reproduced without the use of the IEFPCM model of solvent. The inadequacy of the IEFPCM model may originate in a wrong estimation of the size of the cavity. On the other hand, for benzene solutions, the experimental SOR values are at least three times higher than those calculated by TD-DFT. It is clear that nonelectrostatic effects are more important in this case and that either specific bioxirane-benzene interactions or the chiral arrangement of the benzene molecules surrounding the bioxirane should be taken into account. The former assumption seems unlikely because specific solute-solvent interactions were not observed in water, which is a more favorable solvent for this type of interaction. Therefore, the later assumption seems more likely, since Mukhopadhyay et al. showed in a previous article a significant contribution of the chiral benzene imprint to the calculated SOR of methyloxirane.[18]

3.2.2 – IR and VCD of R-1 and S-1

The IR spectrum of **R-1** in CCl_4 solution is reported in Supporting Information (Figure S7) in the CH stretching and fingerprint regions. A first observation of these spectra reveals the presence of more than 30 (3N-6) modes, indicating the contribution of at least two conformers. The assignment of the different bands has been performed from a potential energy distribution (PED) analysis of the G_+, G_- and *cis* conformers, by using the VEDA program.[36] The internal coordinates needed for calculating the PED are given in Tables S3, whereas PED values for all the vibrations of the three conformers are given in Tables S4-S6. Due to the C_2 symmetry of this dimer-like molecule, the normal modes of vibrations are classified into two symmetry species: in-phase and out-of-phase around the C_2 axis, both modes being active in the IR spectra. Most of the vibrations exhibit a splitting in frequency related to the coupling of the associated oscillators. This splitting is higher than 4 cm^{-1}, except for the methylene stretching modes. It is noteworthy that this splitting depends on the conformation of the molecule which changes the spatial orientation of the transition dipole moments. Figure 4 shows the predicted spectra calculated at the B3LYP/aug-cc-pVTZ level using the IEFPCM model of solvent (CCl_4) for the three conformers. These theoretical spectra can be analyzed to find the bands that are characteristic to each of the three conformers and their intensities can be used to determine the composition of conformers. For example, bands 22 at 1440 cm^{-1} (δC^*H_{ip} iφ + νC^*C^*), 21 at 1381 and 1310 cm^{-1} (δC^*H_{ip} oφ +

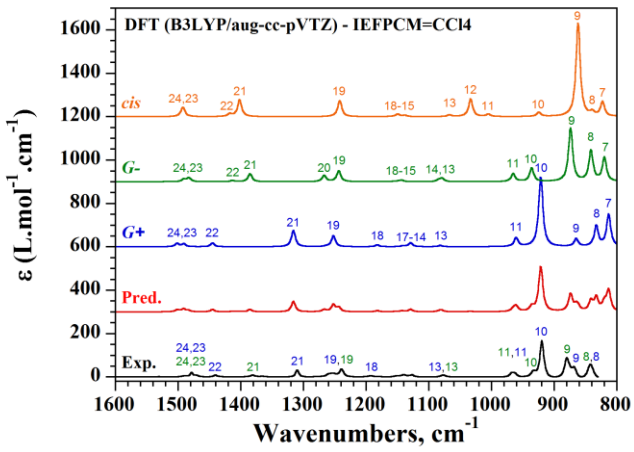

Figure 4. Experimental IR spectrum of **R-1** recorded in CCl_4 solution and predicted spectra calculated at the B3LYP/aug-cc-pVTZ level (IEFPCM=CCl_4) for the G_+, G_-, and *cis* conformers.

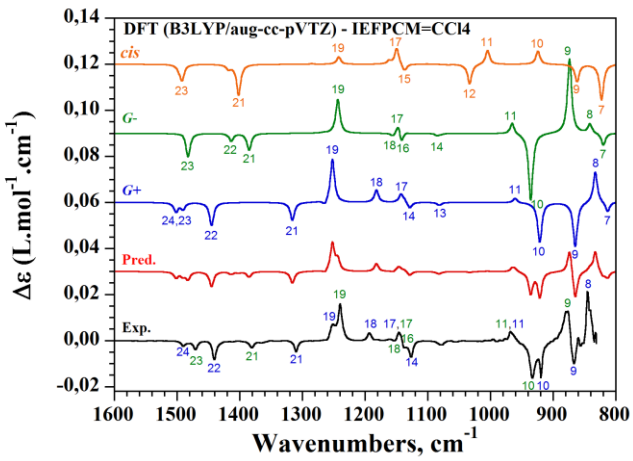

Figure 5. Experimental VCD spectrum of **R-1** recorded in CCl_4 solution and predicted spectra calculated at the B3LYP/aug-cc-pVTZ level (IEFPCM=CCl_4) for the G_+, G_-, and *cis* conformers.

ring breathing), 18 at 1192 cm^{-1} (rocking CH_2 iφ + νC*C*) and 10 at 932 and 920 cm^{-1} (δ_s ring iφ + νC*C*) can be used to determine the relative proportion of the G_+ and G_- conformers. Likewise, band 12 at 1033 cm^{-1} (twisting and rocking CH_2) can be used to determine the proportion of *cis* conformer. The absence of this band on the experimental IR spectrum indicates that the proportion of *cis* conformer is very low in CCl_4 solution. In addition, the very good agreement between the experimental IR spectrum and the predicted spectrum calculated from the averaged population of the three conformers derived from Gibbs energies confirms the higher proportion of the G_+ conformer with respect to the G_- conformer (2/3 : 1/3).

The VCD spectra of the two enantiomers **R-1** and **S-1** recorded in CCl_4 are reported in Supporting Information (Figure S8) in the CH stretching and fingerprint regions. The VCD spectra of the two enantiomers are nearly perfect mirror images, as expected for enantiopure materials. The predicted spectra calculated at the B3LYP/aug-cc-pVTZ level using the IEFPCM model of solvent (CCl_4) for the three conformers and for their averaged population are reported in Figure 5 and are compared to the experimental VCD spectrum of **R-1**. The signs of all the VCD bands observed on the experimental spectrum are perfectly reproduced on the predicted spectrum, allowing the unambiguous determination of the configuration of the sample (ca **R-1**). In addition, the relative intensities of the VCD bands calculated for the predicted spectrum are in good agreement with those observed on the experimental spectrum, except for the band 19 in the 1220-1270 cm^{-1} spectral range.

The VCD spectrum of **R-1** recorded in benzene-d_6 solution exhibits a similar overall shape than the one recorded in CCl_4 solution (see Figure S9 in Supporting Information). This result indicates that the conformer's composition is comparable in the two solutions, as calculated in Table 1. Likewise, there is a great resemblance of the IR spectra recorded in the two solutions (Figure S10 in the Supporting Information). Nevertheless, a closer examination of the IR spectra reveals a slight shift to lower wavenumbers (in the benzene-d_6 solution) of the ring bending bands in the 950 and 820 cm^{-1} region. This feature is certainly due to a particular arrangement of benzene molecules surrounding the bioxirane derivative. This effect could be at the origin of the amazing behavior of the SOR curve of **R-1** in benzene solution.

3.2.3 – Raman and ROA of R-1 and S-1

The ROA spectra of the two enantiomers **R-1** and **S-1** recorded for the neat liquid are reported in Supporting Information (Figure S11). These spectra are perfectly opposite with respect to the baseline, confirming the high enantiomeric excess and the high purity of the two enantiomers. The ROA spectra of **R-1** recorded in several solvents are reported in Figure 6. Similar ROA spectra are observed in CCl_4, cyclohexane and benzene solvents, revealing an identical conformer's population, as suggested by Table 1. Significant spectral differences are noted for water solution and neat liquid; indeed, the bands at 1065 and 804 cm^{-1} increased in water and neat solutions whereas the band at 965 cm^{-1} decreased in nonpolar solvents. Considering the predicted ROA spectra calculated at the B3LYP/aug-cc-pVTZ level for the three conformers (Figure S12 in Supporting Information), all these spectral modifications can be associated with an increase of the G_+ conformer, as expected for polar solvents.

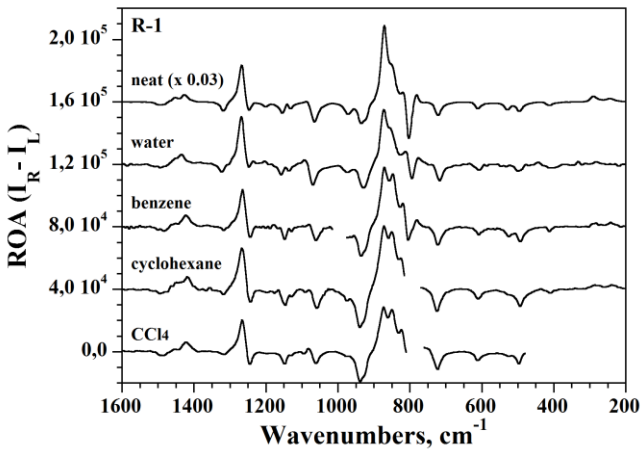

Figure 6. ROA spectra of **R-1** in CCl_4, cyclohexane, benzene, water solutions (0.5 M) and neat liquid.

Conclusion

This article reports the synthesis of the two enantiomers of bioxirane and their chiroptical properties have been studied in various solvents by polarimetry, vibrational circular dichroism (VCD) and Raman optical activity (ROA). Theoretical calculations were performed at the DFT level to make a

conformational analysis of bioxirane and to predict the VCD and ROA spectra for each conformer. The conformational analysis reveals the presence of three conformers (G_+, G_- and *cis*) with Gibbs populations of 51, 44 and 5% for the isolated molecule, respectively. The population of these conformers doesn't change significantly for nonpolar solvents with no permanent dipole moment (CCl_4, cyclohexane and benzene) with Gibbs populations of 64, 32, and 4% for G_+, G_- and *cis* conformers, respectively. For solvents exhibiting higher dielectric constants, the proportion of G_+ conformer increases with respect to the G_- one, whereas the *cis* conformer is close to zero. This conformational analysis predicted by theoretical calculations was supported by VCD and ROA experiments. Moreover, the behavior of the specific optical rotation values with the different solvents was correctly reproduced by the TD-DFT calculations using the polarizable continuum model (PCM), except for the benzene for which explicit solvent model should be necessary. A chiral arrangement of the benzene molecules surrounding the bioxirane could be the cause of this disagreement. This experimental work may be an interesting basis for theoretical chemists that would be interested to investigate in more details the chiroptical properties of the bioxirane derivative with more sophisticated quantum calculation methods (combined QM/MM-MD methods).

Acknowledgements
The authors are indebted to the CNRS (Chemistry Department) and to Région Aquitaine for financial support in VCD and ROA equipments. They also acknowledge computational facilities provided by the MCIA (Mésocentre de Calcul Intensif Aquitain) of the Université de Bordeaux and of the Université de Pau et des Pays de l'Adour, financed by the «Conseil Régional d'Aquitaine» and the French Ministry of Research and Technology.

Supporting information

^{1}H and ^{13}C NMR spectrum of **R-1** and **S-1** in $CDCl_3$ at 298 K. SOR values calculated at the B3LYP/aug-cc-pVTZ level for the G_-, G_+ and *cis* conformers of **R-1**. IR and VCD spectra of **R-1** and **S-1** in CCl_4 and benzene-d_6 solutions. Raman and ROA spectra of **R-1** and **S-1** for the neat liquid. Experimental ROA spectrum of **R-1** recorded in CCl_4 solution and predicted spectra calculated at the B3LYP/aug-cc-pVTZ level (IEFPCM=CCl_4) for the G_+, G_-, and *cis* conformers.

REFERENCES AND NOTES

1. Polavarapu PL, Michalska DF. Mid infrared vibrational circular dichroism in (S)-(–)-epoxypropane. *Mol. Phys.* **1984**, 52:1225-1235.
2. Polavarapu PL, Hess, BA, Schaad LJ. Vibrational spectra of epoxypropane. J. Chem. Phys. **1985**, 82:1705-1710.
3. Kawiecki RW, Delvin F, Stephens PJ, Amos RD. Vibrational circular dichroism of propylene oxide. *J. Phys. Chem.* **1991**, 95:9817-9831.
4. Polavarapu PL, Hecht L, Barron LD. Vibrational Raman optical activity in substituted oxiranes. *J. Phys. Chem.* **1993**, 97:1793-1799.
5. Wang F, Polavarapu PL. Conformational stability of (+)-epichlorohydrin. *J. Phys. Chem. A* **2000**, 104:6189-6196.
6. Losada M, Nguyen P, Xu Y. Solvation of propylene oxide in water: vibrational circular dichroism, optical rotation, and computer simulation studies. *J. Phys. Chem. A* **2008**, 112:5621-5627.
7. Sebestik J, Bour P. Raman optical activity of methyloxirane gas and liquid. *J. Phys. Chem. Lett.* **2011**, 2:498-502.
8. Zehnacker A, Suhm MA. Chirality recognition between neutral molecules in the gas phase. *Angew. Chem. Int. Ed.* **2008**; 47: 6970-6992.
9. Merten C, Bloino J, Barone V, Xu Y. Anharmonicity effects in the vibrational CD spectra of propylene oxide. *J. Phys. Chem. Lett.* **2013**, 4:3424-3428.
10. Bak KL, Devlin FJ, Ashvar CS, Taylor PR, Frisch MJ, Stephens PJ. Ab initio calculation of vibrational circular dichroism spectra using gauge-invariant atomic orbitals. *J. Phys. Chem.* **1995**; 99: 14918-14922.
11 Delvin FJ, Finley JW, Stephens PJ, Frisch MJ. Ab initio calculation of vibrational absorption and circular dichroism spectra using density functional force fields: a comparison of local, nonlocal, and hybrid density functionals. *J. Phys. Chem.* **1995**; 99: 16883-16902.
12. Crawford TD, Tam MC, Abrams ML. The current state ab initio calculations of optical rotation and electronic circular dichroism spectra. *J. Phys. Chem. A* **2007**, 111:12057-12068.
13. Scherrer A, Vuilleumier R, Sebastiani D. Vibrational circular dichroism from ab initio molecular dynamics and nuclear velocity perturbation theory in the liquid phase. *J. Chem. Phys.* **2016**; 145: 084101.
14. Hodecker M, Biczysko M, Dreuw A, Barone V. Simulation of vacuum UV absorption and electronic circular dichroism spectra of methyl oxirane: the role of vibrational effects. *J. Chem. Theory Comput.* **2016**; 12: 2820-2833.
15. Luber S. Raman optical activity spectra from density functional perturbation theory and density-functional-theory-based molecular dynamics. *J. Chem. Theory Comput.* **2017**; 13: 1254-1262.
16. Kongsted J, Pedersen TB, Strange M, Osted A, Hansen AE, Mikkelsen KV, Pawlowski F, Jorgensen P, Hattig P. Coupled cluster calculations of the optical rotation of S-propylene oxide in gas phase and solution. *Chem. Phys. Lett.* **2005**, 401:385-392.
17. Mukhopadhyay P, Zuber G, Goldsmith MR, Wipf P, Beratan DN. Solvent effect on optical rotation: a case study of methyloxirane in water. *ChemPhysChem* **2006**; 7: 2483-2486.
18. Mukhopadhyay P, Zuber G, Wipf P, Beratan DN. Contribution of a solute's chiral solvent imprint to optical rotation. *Angew. Chem. Int. Ed.* **2007**; 119: 6450-6452.
19. Neugebauer J. Induced chirality in achiral media – How theory unravels mysterious solvent effects. *Angew. Chem. Int. Ed.* **2007**; 46: 7738-7740.
20. Egidi F, Barone V, Bloino J, Cappelli C. Towards an accurate modeling of optical rotation for solvated systems: anharmonic vibrational contributions coupled to the polarizable continuum model. *J. Chem. Theory Comput.* **2012**; 8: 585-597.
21. Lipparini F, Egidi F, Cappelli C, Barone V. The optical rotation of methyloxirane in aqueous solution: a never ending story? *J. Chem. Theory Comput.* **2013**; 9: 1880-1884.
22. Match TJ, Crawford TD. Basis set dependence of coupled cluster optical rotation computations. *J. Phys. Chem. A* **2011**, 115:10045-10051.
23. Lindh GD, Match TJ, Crawford TD. The optimized coupled cluster doubles method and optical rotation. *Chem. Phys*. **2012**, 401:125-129.
24. Haghdani S, Aastrand PD, Koch H. Optical rotation from coupled cluster and density functional theory: the role of basis set convergence. *J. Chem. Theory Comput.* **2016**; 12: 535-548.
25. Kumata Y, Furukawa J, Fueno T. The effect of solvents on the optical rotation of propylene oxide. *Bull. Chem. Soc. Jpn.* **1970**, 43:3920-3921.
26. Giorgio E, Rosini C, Viglione RG, Zanasi R. Calculation of the gas phase specific rotation of (S)-propylene oxide at 355 nm. *Chem. Phys. Lett.* **2003**, 376: 452-456.
27. Robbins MA, Devine PN, Oh T. Synthesis of chiral non-racemic diols from (S,S)-1,2,3,4-diepoxybutane:(2S,3S)-dihydroxy-1,4-diphenylbutane. *Org. Synth.* **2004**, 10: 297; **1999**, 76: 101.
28. Buffeteau T, Lagugné-Labarthet F, Sourrisseau, C. Vibrational circular dichroism in general anisotropic thin solid films: measurement and theoretical approach. *Appl. Spectrosc.* **2005**, 59: 732-745.

29. Uncuta C, Bartha E, Gherase D, Teodorescu F, Draghici C, Cavagnat D, Daugey N, Liotard D, Buffeteau T. Conformational equilibria of TADDOL-s in solution investigated by vibrational circular dichroism. *Chirality* **2010**, 22: E115-E122.
30. Daugey N, Brotin T, Vanthuyne N, Cavagnat D, Buffeteau T. Raman optical activity of enantiopure cryptophanes. *J. Phys. Chem. B* **2014**, 118: 5211-5217.
31. Frisch MJ, Trucks GW, Schlegel HB, Scuseria GE, Robb MA, Cheeseman JR, Scalmani G, Barone V, Mennucci B, Petersson GA et al. *Gaussian 09*, revision A.1, Gaussian Inc., Wallingford CT, **2009**.
32. Tomasi J, Mennucci B, Cammi R. Quantum Mechanical Continuum Solvation Models. *Chem. Rev.* **2005**, 105: 2999-3094.
33. Lukasik B, Mikolajczyk M, Bujaczb G, Zurawinski R. Synthesis and the absolute configuration of both enantiomers of 4,5-dihydroxy-3-(formyl)cyclopent-2-enone acetonide as a new chiral building block for prostanoid synthesis. *Org. Biomol. Chem.* **2015**, 13: 807 – 816.
34. Beck A.K, Gysi P, La Vecchia L, Seebach D. (4R,5R)-2,2-dimethyl-α,α,α',α'-tetra(naphth-2-yl)-1,3-dioxolane-4,5-dimethanol from dimethyl tartrate and 2-naphthyl-magnesium bromide. *Org. Synth.* **2004**, 10: 349; **1999**, 76: 12.
35. Kobayashi Y, Kokubo Y, Aisaka T, Saigo K. Hydrogen-bonding sheets in crystals for chirality recognition: synthesis and application of (2*S*,3*S*)-2,3-dihydroxy- and (2*S*,3*S*)-2,3-dibenzyloxy-1,4-bis(hydroxyamino)butanes *Tet. Asymm.* **2008**, 19: 2536 – 2541.
36. Jamróz M.H. Vibrational Energy Distribution Analysis: VEDA 4 program, Warsaw, **2004**.
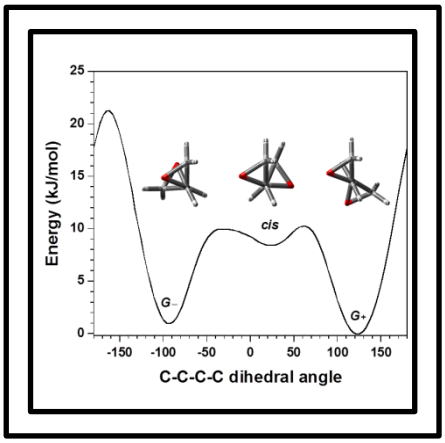
Graphical Abstract